Engineering Structures 272 (2022) 114976

Contents lists available at ScienceDirect

Engineering Structures

journal homepage: www.elsevier.com/locate/engstruct

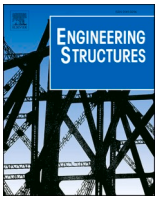

Modular multistable metamaterials with reprogrammable mechanical properties

Jia-Jia Mao [a,*], Shuai Wang [a], Wei Tan [b], Mingchao Liu [c,*]

[a] Beijing Key Laboratory of Nonlinear Vibrations and Strength of Mechanical Structures, Faculty of Materials and Manufacturing, Beijing University of Technology, Beijing 100124, PR China
[b] School of Engineering and Materials Science, Queen Mary University London, Mile End Road, London E1 4NS, UK
[c] School of Mechanical & Aerospace Engineering, Nanyang Technological University, Singapore 639798, Republic of Singapore

ARTICLE INFO

Keywords:
Modular metamaterials
Snap-through
Multistability
Reprogrammability

ABSTRACT

Owing to extensive potential applications in various engineering areas, the multistable metamaterials with remarkable mechanical properties have gained increasing interest from both academia and industry recently. However, the functionality of existing multistable metamaterials is hard to adjust once fabricated. To overcome the limitation, in this paper, we propose an idea of modular multistable metamaterial (MMM) with reprogrammable mechanical properties, which is assembled by unit cells with tunable snap-through behaviours. The unit cell is made by a dismountable bar and a fixed frame containing two bistable curved beams. By inserting the bar with different length into the frame, we can change the shape of curved beams and therefore tune the snap-through behaviour of the unit cell, which lies the foundation of its tunable multistabilities. We evaluate these tunabilities of geometry and mechanical properties of single unit cell by employing theoretical analyses and validate them by numerical simulations. The obtained quantitative results provide us the design guide for assembling of the MMM. We fabricate a certain number of components by 3D printing and assemble them as a unidirectional MMM to examine its reprogrammable macroscopic mechanical behaviours. We firstly investigate the tunable load–displacement responses experimentally and numerically; and then explore the tunable bandgaps through numerical simulations. Finally, we demonstrate the broader possibilities of assembly to form bi- and tri-directional, as well as gradient MMMs. The results presented in this paper have great significance for the design of modular metamaterials and expanding their application prospects in engineering structures.

1. Introduction

Metamaterials are a group of artificial structures or materials constructed by rationally designed building blocks to achieve unusual physical properties not available in natural materials [1]. More crucially, those extraordinary macroscopic properties originate from the microstructural units rather than the material components, which is intrinsically different from conventional engineering materials, and therefore provide us new design schemes for manipulating properties of functional materials at a larger extent [2]. Since the concept of 'metamaterial' is proposed around two decades ago, metamaterials with various extraordinary properties are increasingly studied over the years, including photonic [3,4], acoustic [5,6], electromagnetic [7], thermal [8,9] and mechanical [10–13] metamaterials.

In mechanical metamaterials, unique and programmable mechanical properties, such as shape-morphing, flexibility, tunable Poisson's ratio, tunable stiffness and multi-stability [14–16] can be possessed by engineering their microstructures precisely. As a typical example among those novel architected materials, multistable metamaterials have multiple stable configurations, which render them attractive and rich in various nonlinear behaviours [17], and have been widely studied for their reversible mechanical properties [18–25]. They have been confirmed with excellent abilities of performing large recoverable deformations and achieving notable vibration isolation and energy dissipation through trapping elastic energy in their stable deformed configurations in response to the external loading [26,27]. These advantages promise the potential applications of multistable metamaterials in a wide range of civil engineering applications, including vibration isolation, collision prevention and seismic waveguide, etc [28].

* Corresponding authors.
E-mail addresses: jiajia.mao@bjut.edu.cn (J.-J. Mao), wei.tan@qmul.ac.uk (W. Tan), mingchao.liu@ntu.edu.sg (M. Liu).

https://doi.org/10.1016/j.engstruct.2022.114976
Received 5 July 2022; Received in revised form 24 August 2022; Accepted 13 September 2022
0141-0296/© 2022 Elsevier Ltd. All rights reserved.

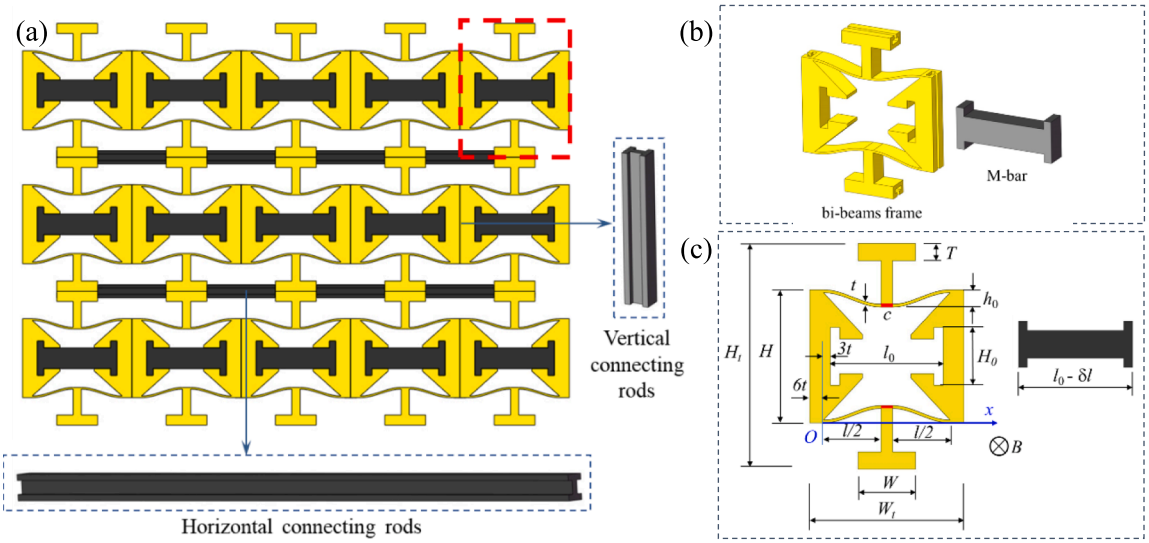

Fig. 1. Schematic diagram of the construction of modular multistable metamaterial (MMM): (a) A MMM with $m \times n$ unit cells together with the schematic of a horizontal and a vertical connecting rod; (b) Oblique view and (c) Front view together with geometric parameters of the single unit cell (left: the variable-width bi-beams frame; and right: the M-bar).

The basic units for constructing multistable metamaterials normally behave bistable, i.e., there are two stable configurations for each unit cell. The sudden transition from one configuration to the other once the applied load reaches a threshold can be referred to as a snap-through buckling instability [29–32]. One of the simplest structures exhibiting bistability is a curved elastic beam, which could be either intrinsically curved or be formed by axially compressing a straight beam. The pioneering theoretical model to analyse the bistable behaviour of an initially curved beam was developed by Qiu et al. [33], and it revealed that the critical condition for the bistability of the initially curved beam only depends on its height-to-thickness ratio once the second mode is eliminated.

Taking advantages of the elastic snap-through of initially curved beams, Restrepo et al. [18] introduced the concept of phase transformation into periodic cellular structures consisting of unit cells with multiple stable configurations. In the meantime, Rafsanjani et al. [20] embedded the snap-through buckling into multistable metamaterials under tension. Shan et al. [22] designed multistable metamaterial that performs controlled trapping of elastic energy for impact by using bistable tilted beams. All of these developments raise up the emergence of studies on multistable metamaterials. As typical examples, inspired by geometric motifs in ancient architectures, Rafsanjani and Pasini [34] designed a class of switchable architected materials exhibiting auxeticity and bistability simultaneously. More recently, Zhang et al. [35] and Yang and Ma [36,37] proposed a series of 2D and 3D multistable metamaterials with zero Poisson's ratio and negative stiffness, which exhibit improved mechanical behaviours, such as enhanced energy absorption and strengthened structural reliability. In addition, multistable metamaterials also demonstrated anomalous dispersion characteristics, which provide ability of elastic wave manipulation and vibration isolation. For example, Wang et al. [38] and Ren et al. [39] demonstrated that the multistable metamaterials can be harnessed for tuning bandgaps. More works about the multistable metamaterials are summarized in the comprehensive review papers [14,40].

All the aforementioned results demonstrated that multistable metamaterials have huge application prospects in engineering and science. However, the predetermined functionality of multistable metamaterials normally cannot be altered once fabricated. Recently, several preliminary attempts have been presented. For example, several multistable metamaterials with tunable mechanical responses through controlling the external stimuli, such as lateral confinement [41], gas pressure [42], environment temperature [43,44] and magnetic interaction [45], have been presented. Although the properties of those multistable *meta*-materials can be tuned after fabrication, the tuned behaviours cannot be maintained once the external stimuli are removed. To overcome this challenge, a modular multistable *meta*-material (MMM) with reprogrammable mechanical properties is proposed in this paper by assembling elaborately designed unit cells with the tunable mutistable mechanism. The tunable unit cell is composed by a bi-beams frame with variable width and a middle-bar (M-bar). A theoretical model is developed to describe the tunable geometric and mechanical properties of the unit cell, and it is validated by finite element method (FEM) simulations. Furthermore, FEM simulations and experimental tests combined with 3D printing are used to analyse the reprogrammable mechanical properties, i.e., load–displacement responses and tunable bandgaps, of the assembled MMMs. The proposed MMMs are promising to realize reusable, portable and tunable energy absorbers in many fields, especially in civil engineering, protecting delicate objects during piling on different geologies.

2. Design and fabrication of MMM

Fig. 1 shows the schematic diagram of the construction of the proposed modular multistable metamaterial (MMM) with $m \times n$ unit cells (building blocks), where m and n are the number of unit cells in the horizontal and vertical directions, respectively. These unit cells are connected by horizontal and vertical rigid connecting rods (see Fig. 1 (a)). The unit cell consisting of a frame with two curved beams together with a slot in the middle (we refer it as bi-beams frame, see the yellow part) and a rigid middle-bar (M-bar, see the gray part, which can be inserted into the slot) is presented in Fig. 1(b) and (c), corresponding to the oblique and front views, respectively. Fig. 1(c) also illustrates the main geometric parameters of the bi-beams frame and the M-bar. Two curved beams within the frame have the same height h_0 and thickness t. H_t and W_t are the total height and width of the bi-beams frame, respectively, which can be varied by inserting the M-bar with different length $l_0 - \delta l$. B is the out-of-plane thickness (or depth) of the frame. Except for these two curved beams, the rest parts of the bi-beams frame and the M-bar can be considered as rigid when subjecting external load since their thicknesses are much larger than t. We also introduced the connecting platform with length c located in the middle of the curved beam (see the red part in Fig. 1(c)), which is able to constrain the second

Table 1
Geometrical parameters used (unit: mm).

H_t	H	H_0	h_0	t	T	W_t	W	c	l	l_0
78	46	20	5	1	6	67	25	5	50	49

buckling mode mechanically when the curved beam snaps from one configuration to another [36].

All the components, including the bi-beam frame, the M-bar and the horizontal and vertical connecting rods, are fabricated through additive manufacturing (3D printing). The geometries (CAD model) of the printed structures are created by SolidWorks. The bi-beams frames are printed with thermoplastic polyurethane (TPU with Young's modulus E = 180 MPa) using Fused Deposition Modeling (FDM) technology (HORI H1, Beijing Huitianwei Technology Co., Ltd., China). Nylon 7100 (with E = 1.0 GPa) is chosen for printing the connecting rods and M-bars through Selective Laser Sintering (SLS) technology (WeNext Technology Co., Ltd, China). Since Nylon 7100 is much stiffer than TPU, the connecting rods and M-bars can be considered as rigid. Three different lengths of the M-bars $l_0 - \delta l$ (δl = 0, 2, 4 mm) are considered. The detailed geometrical parameters for the specimens are given in Table 1.

Previous works have indicated that the key parameter for describing the mechanical behaviours, especially the threshold of bistability and the load–displacement relationship, of the curved beam is the height-to-thickness ratio $Q = h_0/t$ [33]. For the unit cell proposed here, when inserting a M-bar with length $l_0 - \delta l$ which is shorter than original length of the slot built-in the bi-beams frame l_0, the height of two curved beams changes synchronously and equally. Hence, the height-to-thickness ratio Q is varied accordingly, and therefore, both the geometry and mechanical response of the unit cell can be tuned. Assembling these tunable unit cells with horizontal and vertical connecting rods, MMMs with programmable mechanical properties can be formed, as shown in Fig. 1 (a).

It is noted that the snap-through behaviours of the bistable curved beam accompany with large recoverable deformation along vertical direction, zero horizontal displacement, as well as negative stiffness under displacement control [33]. Hence, the MMM assembled by the designed unit cells can achieve multistability, zero Poisson's ratio and negative stiffness simultaneously. As the multiple metamaterial properties of the MMMs significantly depend on the snap-through behaviours, we shall start to focus on the mechanical behaviours of the single unit cell; and then investigate the macroscopic (effective) mechanical properties of the assembled MMM in the following sections via theoretical analysis, FEM simulations and physical experiments.

3. Numerical and experimental methods

3.1. The FEM simulations

FEM simulations are performed using the ABAQUS Explicit to analyse the mechanical behaviours of the proposed curved beams, unit cells and MMMs. The geometries and physical parameters of FEM models are in accordance with the experimental specimens. Neo-Hookean hyperelastic (C_{10} = 30.29, D_{10} = 0.00025) and linear elastic (E = 1 GPa, μ = 0.3) constitutive models are adopted for the bi-beams frames and M-bars, respectively. The geometric nonlinearity is considered, and the models are meshed with 8-node reduced integration solid elements (C3D8R). To ensure the computational accuracy, mesh sensitivity analyses are carried out for the snap-through behaviour of a curved beam, which is fixed at two ends and subjected to a normal load at the central part. As shown in Fig. A1 in Appendix A, mesh size 0.50 mm is enough for the calculation accuracy. Hence, we adopt it for all the simulations.

To simulate the deformation of unit cells, the "Tie" function is used to describe the connections between the M-bar and the bi-beams frame. Changing length of the M-bar is realised by introducing orthotropic thermal expansion coefficients (α_{11} = 0.1/ °C and α_{22} = α_{33} = 0) for the M-bar; whilst other parts in the model are insensitive to temperature change. The variations of the length, δl = 0, 2 and 4 mm, are achieved by changing the temperature with ΔT = 0, –0.41 and –0.82 °C. For the deformation behaviours of the MMM, taking the case with δl = 4 as an example, two steps are introduced in the simulation: in the first step, the temperature change of $\Delta T = -0.82$°C is applied to shorten the length of the M-bar to the certain value, $l_0 - \delta l$; in the second step, the bottom edge of the MMM is fixed, and the vertical displacement is applied to the top edge of the MMM through a reference point while fixing horizontal displacement as zero (see Movie S1 in Supporting Information for more details).

3.2. The experimental tests

Similar to the illustration in Fig. 1(a), as a typical example, the MMM with 5 × 3 unit cells can be assembled by the horizontal and vertical rigid connecting rods (details of the assembling process can be found in Movie S2 in the Supporting Information). The Zwick Z005 testing machine is used to measure the macroscopic mechanical behaviours, more specifically, the load–displacement (f-d) responses, of the assembled MMMs inserted with M-bar with different lengths (δl=0, 2 and 4 mm) according to the central uniaxial tensile tests. The displacement load is applied at a rate 5 mm/min (ensuring a quasi-static loading, see Movie S3 in Supporting Information) and stopped when all the curved beams snapped. We need to note here that we only replace the M-bars but keep using the same bi-beam frame when we measure the MMMs with different δl to investigate the reprogrammable mechanical properties of the proposed MMMs. Besides, we also quantify the mechanical properties of the 3D-printed TPU through the tensile test of the dumbbell specimens according to the standard ASTM D412-16. The Young's modulus is measured as E = 180 MPa.

4. Tunable mechanical behaviours of single unit cell

4.1. The curved beam

4.1.1. The geometric property

The mechanical behaviours of the unit cell are highly depending on its geometric parameters. More particularly, they are determined by the geometry of the curved beam within the bi-beams frame. Considering one curved beam within the bi-beams frame (see Fig. 1(c)) and ignoring the connecting platform, its shape can be given by [33]

$$w_0 = -\frac{h_0}{2}\left[1-\cos\left(\frac{2\pi x}{l}\right)\right], \quad x \in [0, l] \tag{1}$$

and the arc-length of the curved beam can be expressed as

$$s_0 = \int_0^l \sqrt{1+\left(\frac{dw_0}{dx}\right)^2}\,dx \approx \int_0^l \left[1+\frac{1}{2}\left(\frac{dw_0}{dx}\right)^2\right]dx \tag{2}$$

It is assumed that the varying width δl of the bi-beams frame only affects the height $h = h_0 + \delta h$ of the curved beam but has no influence on its shape and the arc-length. The resulted shape and arc-length of the curved beam can be written as

$$w = -\frac{h_0+\delta h}{2}\left[1-\cos\left(\frac{2\pi x}{l-\delta l}\right)\right], \quad x \in [0, l-\delta l] \tag{3}$$

and

$$s = \int_0^{l-\delta l} \sqrt{1+\left(\frac{dw}{dx}\right)^2}\,dx \approx \int_0^{l-\delta l} \left[1+\frac{1}{2}\left(\frac{dw}{dx}\right)^2\right]dx \tag{4}$$

Let

$$s = s_0 \tag{5}$$

the variation of the height δh and the height-to-thickness ratio Q =

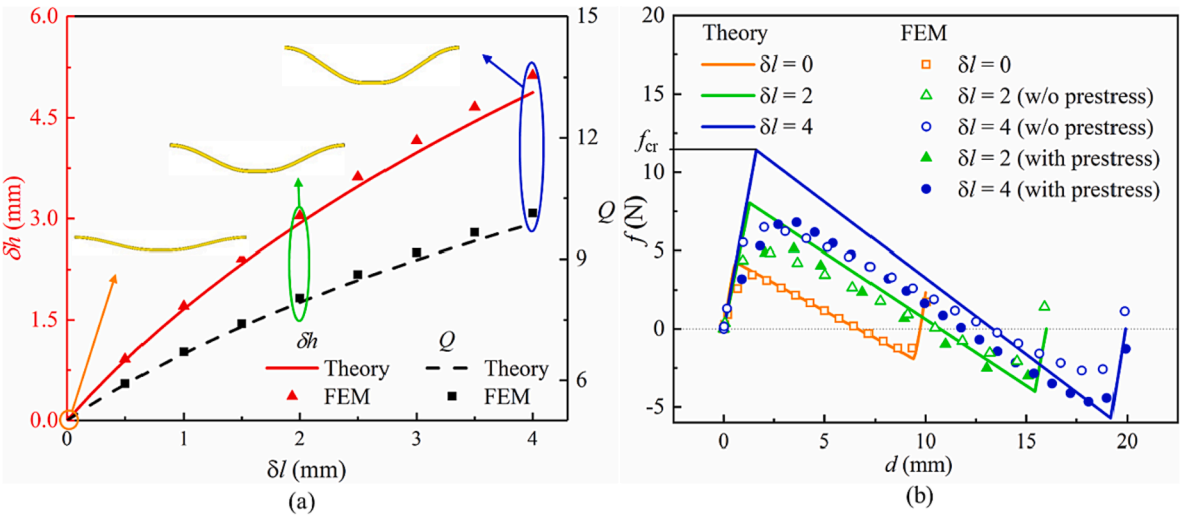

Fig. 2. Tunable geometric properties and mutistable mechanism of the curved beam: (a) Effect of varying width of bi-beams frame (δl) on the variation of height (δh) and the corresponding height-to-thickness ratio (Q) of curved beams; and (b) normal load–displacement (f-d) curves for one of the curved beams with different widths of bi-beams frames ($l_0 - \delta l$).

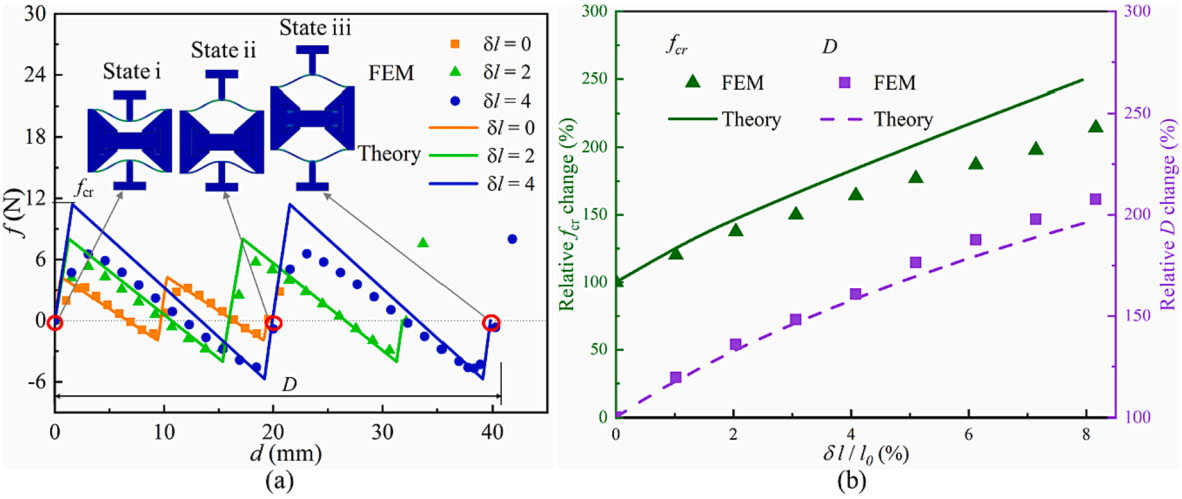

Fig. 3. Tunable snap-through behaviour of the single unit cell: (a) f-d curves for single unit cell with different values of δl, and snapshots of the corresponding stable configurations for the case with $\delta l = 4$; (b) variations of the threshold load f_{cr} and the total displacement D as a function of the normalized width of unit cell $\delta l/l_0$.

$(h_0 + \delta h)/t$ caused by the change in width δl of the bi-beams frame can be calculated. The corresponding results for the curved beam with $l =$ 50mm, $c = 5$mm, $h_0 = 5$mm and $t = 1$mm are given in Fig. 2(a). As a comparison, results obtained from FEM simulations are also included in Fig. 2(a). It shows that the adjustments of both δh and Q corresponding to δl can be predicted accurately by the theoretical model.

4.1.2. The mutistable mechanism

For an intrinsically curved beam with clamped–clamped boundaries, there are two stable states (configurations) when the height-to-thickness ratio satisfies $Q > 2.31$ [33]; Otherwise, the second state is unstable. Since the main propose of this work is to consider the multistable metamaterial by using the curved beam as a fundamental component, we shall focus on the bistable situation. For a bistable curved beam subjected to a normal load, f, at the central point (or alternatively the displacement load, d, which corresponds to the reaction force f), it can switch to the second stable configuration from its original configuration (naturally stable) via snap-through buckling when the load reaches the threshold f_{cr}.

Qiu et al. [33] indicated that the load–displacement (f-d) curve of a curved beam during the snap-through transition has both positive and negative stiffness stages. When the second mode is constrained, by normalizing the normal load and the displacement as $F = fl^3/(EIh)$ and $\Delta = d/h$ respectively, their relationship can be obtained [33] as

$$F = \begin{cases} \dfrac{3\pi^4 Q^2}{2}\Delta\left(\Delta - \dfrac{3}{2} + \sqrt{\dfrac{1}{4} - \dfrac{4}{3Q^2}}\right)\left(\Delta - \dfrac{3}{2} - \sqrt{\dfrac{1}{4} - \dfrac{4}{3Q^2}}\right) \\ 8\pi^4 - 6\pi^4\Delta \end{cases} \tag{6}$$

It is worth noting here that the normalized force–displacement (F-Δ) curve is a hybrid curve that switches between curves given by two subformulas in Eq. (6). More specifically, in the full range of loading (i.e. $0 \le \Delta \le 2$, which is corresponding to $0 \le d \le 2\,h$), the first subformula describes the two sections with positive stiffness at both ends of the F-Δ curve, which depends on the height-to-thickness ratio Q, and the second subformula predicts a straight line connecting those two sections [33], as shown in Fig. 2(b). Therefore, the snap-through behaviour of the curved beam is directly related to Q. By changing the width of the bi-beams frame, which can be realized by inserting a M-bar with length $l_0 - \delta l$, curved beams within the unit cell are stressed, and the height-to-

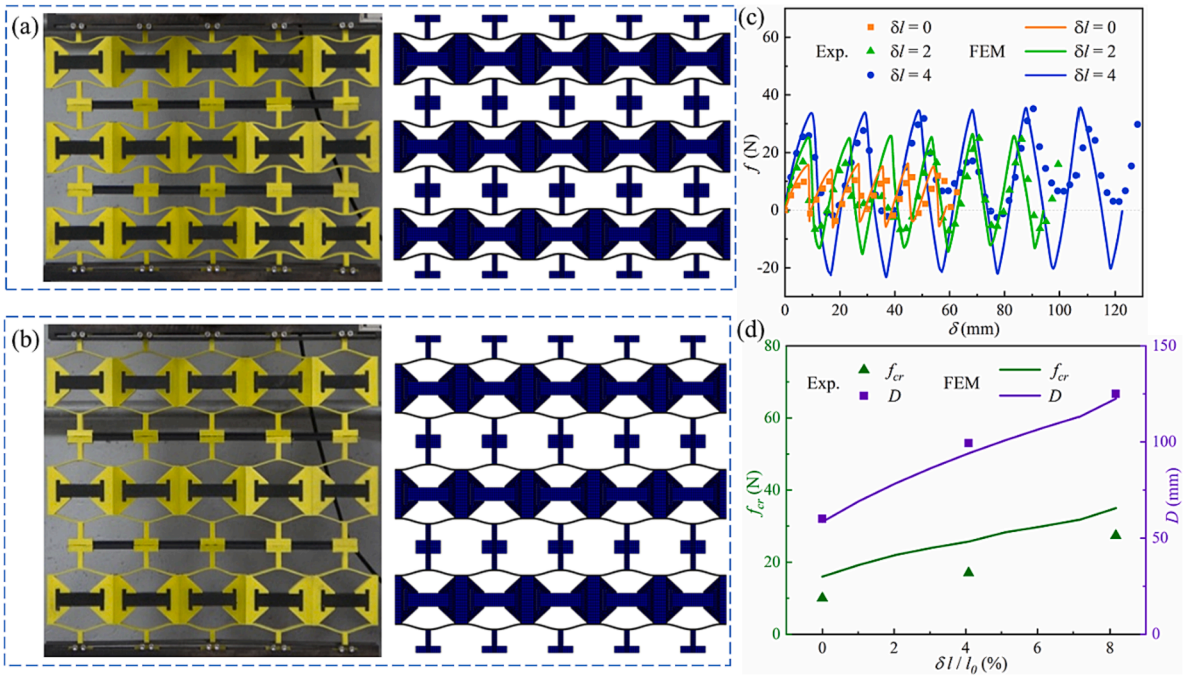

Fig. 4. Reprogrammable mechanical properties of MMMs: Snapshots of (a) the fully folded state and (b) the fully deployed state for the assembled MMM (with 5 × 3 unit cells) with $\delta l = 0$ in both experiments and FEM simulations; (c) *f-d* curves for the MMM with different values of δl; and (d) Critical load f_{cr} and the total displacement D of the MMM as a function of the normalized width of the unit cell $\delta l/l_0$.

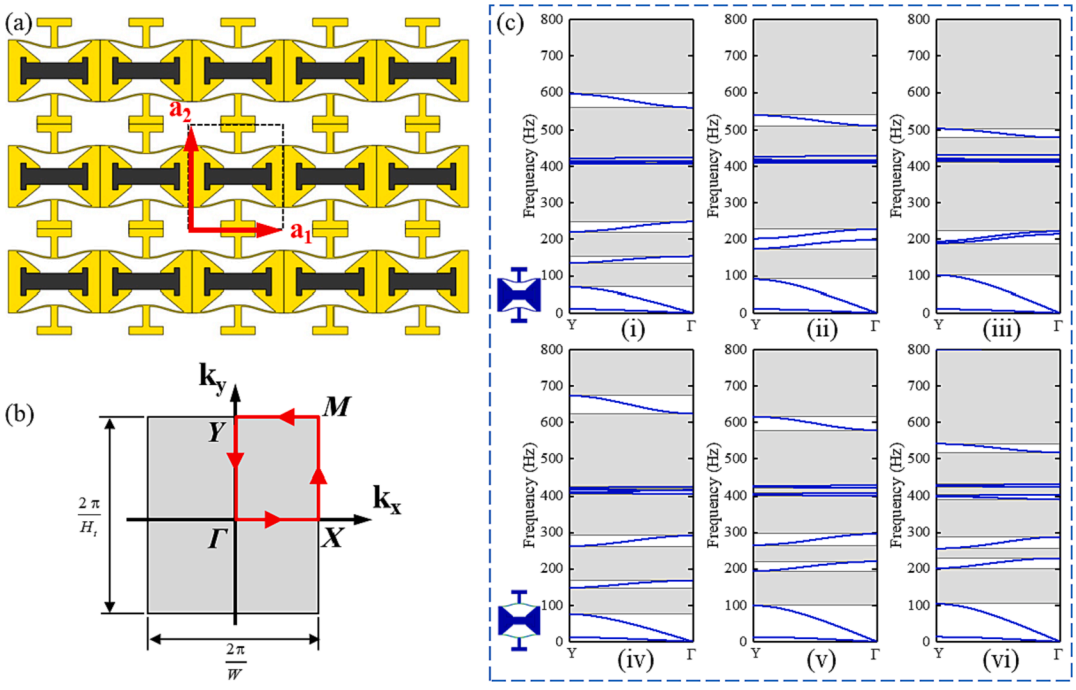

Fig. 5. Band structure analysis of the unidirectional MMM: (a) Schematic of the MMM together with the direct lattice vectors; (b) Reciprocal lattice vectors together with the irreducible Brillouin zone; and (c) Band structures of the fully folded states (i-iii) and fully deployed states (iv-vi) with varying δl ($\delta l =$ 0, 2 and 4 mm).

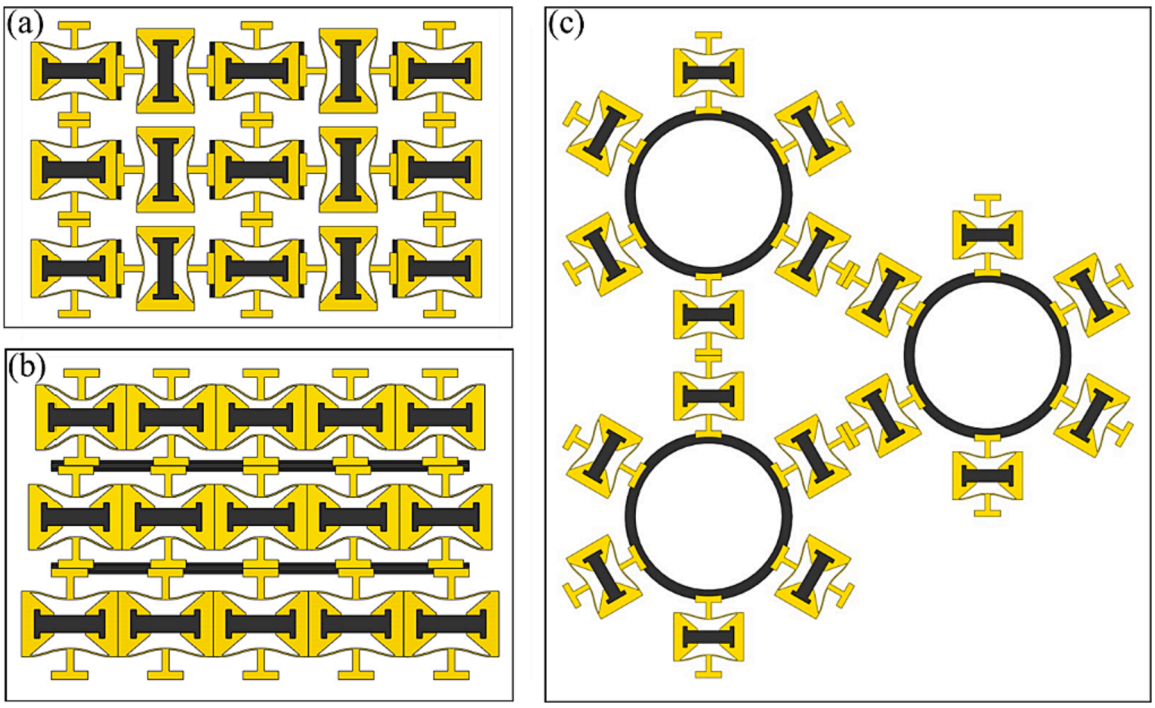

Fig. 6. Additional assembling arrangements of MMMs. (a) Bi-directional, (b) Gradient and (c) Tri-directional MMMs.

thickness ratio Q varies correspondingly (Fig. 2(a)), which results in the variation of the relationship between F and Δ.

According to the normalization implemented before, the dimensional values of the normal load and the displacement can be obtained as $f = F{\cdot}EIh/l^3$ and $d = \Delta{\cdot}h$, respectively. Obviously, the values of f and d for the unit cells can also be obtained through Eq. (6). Fig. 2(b) presents the effect of changing δl on the f-d curves of the curved beams. One can clearly see that the f-d relationship strongly depends on the value of δl. We can expect that the macroscopic mechanical properties of MMMs can be programmed by assembling multiple unit cells inserted with M-bars of particular length in a desired arrangement. More importantly, the M-bar is dismountable, which indicates that we can reprogram the macroscopic properties of the MMM by replacing M-bars with different lengths.

It is worth noting that the theoretical result given by Eq. (6) is essentially geometrical: the normalized normal load F only depends on the normalized displacement Δ, and there is no prestress (i.e. the residual stress generated in the assembly process) involved in — this is only exact for the preformed beam with intrinsic curvature. For those cases we present here, the stress-free condition satisfies just for the case with $\delta l = 0$. However, when we change the width of the bi-beams frame by $\delta l > 0$, the curved beams within the bi-beams frame will be stressed, and larger δl corresponds to larger prestress.

To evaluate the effect of prestress on the mechanical response of the curved beam, we introduce the prestress into curved beams by compressing them to change their length by δl in FEM simulations, which corresponds to the shape-change induced in the assembly process of inserting the M-bar with length $l_0 - \delta l$ into the bi-beams frame. Therefore, the prestress has been embedded into the generated curved beams with different δl, and the corresponding f-d relationships are measured, as shown in Fig. 2(b) by solid symbols. For comparison, we also measure the f-d relationships of curved beams with the same shape (as preformed) but without prestress in FEM simulations (the corresponding FEM models with $\delta l = 4$ are presented in Fig. A2 in Appendix A). The results are shown in Fig. 2(b) by hollow symbols. For the same δl, one can find that there is minor difference between FEM results with and without prestress. It indicates that the effect of prestress on the snap-through behaviour is minor and can be ignored for those cases we are considering here.

Besides, there are some differences between the theoretical and FEM results in Fig. 2(b), which increase with the increase of δl, i.e., the decreasing length of the curved beam. The theoretical analyses used here are referred to Qiu et al. [33], in which the curved beam is treated as a Euler beam. Actually, even though the curved beam has a small thickness, it behaves more like a Timoshenko beam as its length isn't large enough and the shear deformation is non-negligible. The differences here are partly introduced by the difference between the Euler theory and the Timoshenko theory. It is also illustrated by Hua et al. [46] that increasing the length of the curved beam can reduce the differences between the theoretical and FEM results. Although the differences exist, the snap-through behaviours of the curved beam and its tunability can be predicted by Eq. with acceptable error once the corresponding height-to-thickness ratio Q is calculated from Eq. with a certain δl. Now we shall move on to investigate the mechanical behaviours of unit cells.

4.2. The unit cell

The results in Section 4.1 indicate that the mechanical behaviours of the single unit cell can be tuned by changing the width of the bi-beams frame. It can be experimentally realized by inserting M-bar with different length $l_0 - \delta l$, as presented in Section 3.2; and numerically mimicked by setting orthotropic thermal expansion of the M-bar in FEM simulation, see Section 3.1 for more details. The f-d curves of unit cells with inserted M-bar of varying length in FEM simulations are plotted in Fig. 3(a). Obviously, the multistable response of unit cells can be significantly modulated by using M-bars with different lengths. Each curve has three stages with positive stiffness, corresponding to three states of the unit cell, i.e., (i) the fully folded state, (ii) the partially deployed state and (iii) the fully deployed state. The corresponding configurations of those states are shown in the insert of Fig. 3(a).

Comparing the f-d curves of unit cells with different δl, we can find that both the threshold of the normal load f_{cr} for the first snap-through

buckling of the single unit cell and the total displacement D for the single unit cell deforming from state (i) to state (iii) are significantly tuned by changing δl. The measured values of f_{cr} and D for unit cells inserted M-bar with different lengths are plotted as a function of the normalized varying width $\delta l/l_0$ by symbols in Fig. 3(b), which agree well with the theoretical predictions (i.e., the corresponding solid and dash lines). Quantitatively, for the length of M-bar varies only 8%, the increases of f_{cr} and D can be achieved by 115% and 105%, respectively. These results are impressive and indicate that mechanical behaviours of unit cell are tunable and reprogrammable. Now we shall move on to consider the macroscopic properties of MMM assembled with multiple unit cells.

5. Reprogrammable mechanical properties of MMMs

As we have shown in Section 4 that the mechanical properties of single units are tunable, the macroscopic mechanical properties of MMMs are expected to be programmed by assembling multiple unit cells with the dismountable M-bars in a particular arrangement. We demonstrate the reprogrammable mechanical properties of the proposed MMMs in detailed below.

5.1. The load–displacement responses

According to the central uniaxial tensile tests (from the original configuration (fully folded state) with $\delta l = 0$ as shown in Fig. 4(a) to all the fully deployed state in Fig. 4(b), see Section 3.2 for details), the *f-d* curves of MMMs inserting with M-bars of different lengths (δl=0, 2 and 4 mm) are plotted in Fig. 4(c) by using solid symbols. It is seen that the *f-d* curves can be significantly modulated by choosing M-bars with different length, which indicates that the MMMs are reprogrammable for desired mechanical properties. The *f-d* relationships for the cases with different values of δl obtained from FEM simulations (see Section 3.1 for details) are plotted in Fig. 4(c) by solid lines. It is clearly seen that the FEM simulation results agree with the experimental results qualitatively well. These *f-d* curves for MMMs with different δl also indicate that the threshold load of snap-through buckling, f_{cr}, as well as the total displacement, D, are programmable by choosing M-bar with different length. More quantitatively, we plot both the values of f_{cr} and D obtained from FEM simulations as a function of δl in Fig. 4(d). One can notice that f_{cr} and D can be increased by 118% and 108%, respectively, for the length of M-bar varies only 8%.

5.2. Tunable bandgaps for elastic waves

The proposed MMMs possess reprogrammable snap-through behaviours on the basis of configuration evolution induced by replacing M-bar with different lengths. Because of the tunability of geometric configurations and correspondingly generated pre-stress, the MMMs show the potential capability of manipulating elastic waves and vibration isolation [38,39]. As the aforementioned MMM is multistable along and only along the vertical direction, it is referred as unidirectional MMM. We choose the unidirectional MMM (see Fig. 5(a)) as an example to investigate the manipulation of its band structures of waves propagating by changing their states from fully folded to fully deployed; and/or replacing M-bars with different length $l_0 - \delta l$.

The Solid Mechanics module of COMSOL Multiphysics is employed to analyse the bandgap structures of the unit cells with different δl. Both the fully folded state and the fully deployed state are considered. The geometric models of the fully folded state are obtained from ABAQUS Explicit and imported into COMSOL directly; while the fully deployed geometric models are obtained through applying tension to the fully folded state by adding a load step before calculating the band structure. Floquet periodic boundary is applied to the unit cell. The densities of TPU and nylon 7100 are 1250 Kg/m^3 and 1000 Kg/m^3, respectively. Taking the fully folded unit cell with $\delta l = 0$ as an example, according to the periodic distribution of microstructures, the basic lattice vectors of the proposed MMM are defined as ($\boldsymbol{a_1}$, $\boldsymbol{a_2}$), which are corresponding to the unit cell of the MMM, as shown in Fig. 5(a), which can characterize the direct lattice. The first Brillouin zone is defined by the reciprocal lattice vectors ($\boldsymbol{k_x}$, $\boldsymbol{k_y}$), and the irreducible Brillouin zone (IBZ) is marked by red arrows in Fig. 5(b), departing from Y, going through Γ, X and M successively, and finally back to Y. The dispersion relation can be computed in the reciprocal space by varying wave number k along the first Brillouin Zone.

Since the MMMs we considered here are unidirectional, the waves propagating along the vertical direction is dominance. We calculate the band structures of MMMs with different δl along the vertical direction. The band structures of fully folded states (see (i)-(iii) in Fig. 5(c)) and fully deployed states ((iv)-(vi) in Fig. 5(c)) of the MMMs with $\delta l = 0$, 2 and 4 mm are plotted. As we can see from Fig. 5(c), the band structures of the MMM can be visibly adjusted by either controlling the states (from folded state to deployed state) or changing the geometries (by inserting M-bars with different lengths).

6. Additional assembling arrangements of MMMs

Until now, the reprogrammable mechanical properties of the proposed MMM are illustrated and validated systematically. It can be expected naturally that, apart from the unidirectional MMM presented above, the designed unit cells can be assembled in more plentiful ways to form multistable metamaterials performing different mechanical properties in multi-directions and/or with gradient. Here we would demonstrate several assembling arrangements as illustration.

As shown in Fig. 6(a), rotating the second and fourth columns of the unit cells comparing with the unidirectional MMM (see Fig. 1(a)), the resulting structure will behave with tunable mechanical properties along both horizontal and vertical directions, which can be referred as bi-directional MMM. In addition, a gradient MMM can be obtained by inserting M-bars with different lengths in different rows of unit cells (see Fig. 6(b)). It is expected that the load–displacement curve of the gradient MMM will vary stepwise. It is worth noting that introducing M-bars with different lengths into the bi-directional (Fig. 6(a)) MMMs can also achieve aperiodic structures with nonuniform load–displacement curves along two different directions. Both these two MMMs are orthogonal and assembled with straight connecting rods. Connecting unit cells with circular rings as shown in Fig. 6(c), a nonorthogonal MMM containing three axes of symmetry, namely tri-directional MMM, is assembled.

Obviously, except for the bi-directional, gradient, and tri-directional MMMs proposed above, more complex orthogonal and nonorthogonal MMMs can be formed with the rational designed unit cells to realize more abundantly reprogrammable mechanical properties and bandgaps, and hence develop the potential applications of the MMMs; we shall leave a detailed analysis of the mechanical behaviours of those complex MMMs for a future study.

7. Conclusion

To achieve the reprogrammable mechanical properties of multistable metamaterials, we proposed an idea of modular structures by assembling 3D printed components. More specifically, we designed the unit cell consisting of a bi-beams frame and a M-Bar and with tunable snap-through behaviours, in which the width of the bi-beams frame can be adjusted by inserting M-bar with different length. MMMs were formed through assembling unit cells by connecting rods. Both theoretical

analyses and FEM simulations are adopted to explore the tunable multistable mechanism of the unit cell. The effects of M-bars with different lengths on the load–displacement curves and bandgaps of the assembled MMMs are investigated through FEM simulations and experimental tests combined with 3D printing. Main conclusions can be obtained as bellow:

(1) The multistable behaviours of designed unit cell can be adjusted by inserting M-bar with different length and predicted theoretically.
(2) The effective mechanical properties (both the load–displacement curves and the bandgaps of elastic wave) of assembled unidirectional MMMs have been demonstrated as reprogrammable by replacing M-bars with different lengths.
(3) In addition to the unidirectional MMM, the bi-directional, tri-directional and gradient MMMs can also be assembled by connecting designed unit cells in different arrangements.

CRediT authorship contribution statement

Jia-Jia Mao: Conceptualization, Investigation, Formal analysis, Writing – original draft, Funding acquisition, Supervision. **Shuai Wang:** Software, Investigation, Data curation, Writing – original draft. **Wei Tan:** Visualization, Writing – review & editing. **Mingchao Liu:** Conceptualization, Validation, Formal analysis, Methodology, Writing – review & editing.

Declaration of Competing Interest

The authors declare that they have no known competing financial interests or personal relationships that could have appeared to influence the work reported in this paper.

Data availability

Data will be made available on request.

Acknowledgements

This work was supported by the National Natural Science Foundation of China (12172012, 11802005), the General Program of Science and Technology Development Project of Beijing Municipal Education Commission (KM201910005035), the EPSRC (grant EP/V049259/1), European Commission Graphene Flagship Core Project 3 (GrapheneCore3) under grant No. 881603, and the Nanyang Technological University via the Presidential Postdoctoral Fellowship.

Appendix A

Fig. A1 and Fig. A2

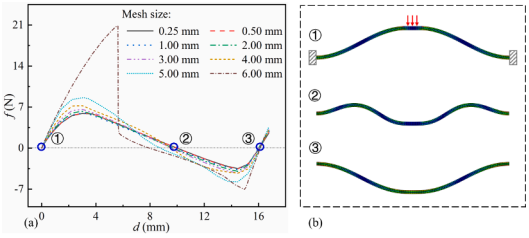

Fig. A1. (a) Effect of mesh size on the *f-d* relationship of the curved beam and (b) the FEM model ($\delta l = 2$) at different states with mesh size 0.50 mm.

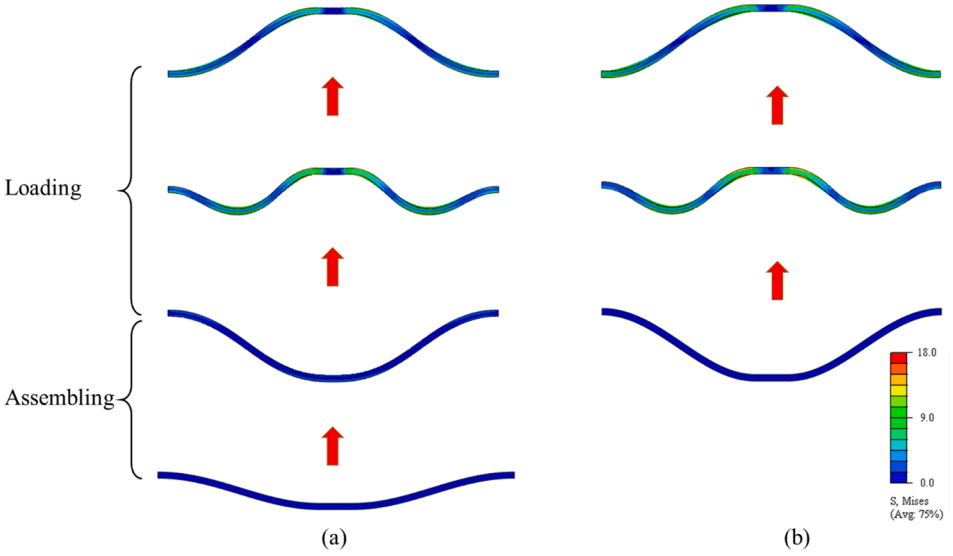

Fig. A2. The FEM model and deformation process of (a) the curved beam with $\delta l = 4$, which is deformed from a stress-free state (with $\delta l = 0$) and embedded with prestress; and (b) the curved beam with the same shape as the case with $\delta l = 4$ but without prestress.

Appendix B. Supplementary data

Supplementary data to this article can be found online at https://doi.org/10.1016/j.engstruct.2022.114976.

References

[1] Liu YM, Zhang X. Metamaterials: a new frontier of science and technology. Chem Soc Rev 2011;40:2494–507.
[2] Kadic M, Milton GW, van Hecke M, Wegener M. 3D metamaterials. Nat Rev Phys 2019;1(3):198–210.
[3] Smith DR, Pendry JB, Wiltshire MCK. Metamaterials and negative refractive index. Science 2004;305(5685):788–92.
[4] Huang TT, Ren X, Zeng Yi, Zhang Yi, Luo C, Zhang XY, et al. Based on auxetic foam: A novel type of seismic metamaterial for Lamb waves. Eng Struct 2021;246:112976.
[5] Zhang S, Xia CG, Fang N. Broadband Acoustic Cloak for Ultrasound Waves. Phys Rev Lett 2011;106:024301.
[6] Ma T-X, Fan Q-S, Zhang C, Wang Y-S. Flexural wave energy harvesting by the topological interface state of a phononic crystal beam. Extreme Mech Lett 2022;50:101578.
[7] Schurig D, Mock JJ, Justice BJ, Cummer SA, Pendry JB, Starr AF, et al. Metamaterial electromagnetic cloak at microwave frequencies. Science 2006;314(5801):977–80.
[8] Wang Q, Jackson JA, Ge Q, Hopkins JB, Spadaccini CM, Fang NX. Lightweight Mechanical Metamaterials with Tunable Negative Thermal Expansion. Phys Rev Lett 2016;117:175901.
[9] Zhu H, Fan T, Peng Q, Zhang Di. Giant Thermal Expansion in 2D and 3D Cellular Materials. Adv Mater 2018;30(18):1705048.
[10] Siéfert E, Reyssat E, Bico J, Roman B. Bio-inspired pneumatic shape-morphing elastomers. Nat Mater 2019;18(1):24–8.
[11] Liu MC, Domino L, Vella D. Tapered elasticae as a route for axisymmetric morphing structures. Soft Matter 2020;16:7739–50.
[12] Zhang Y, Velay-Lizancos M, Restrepo D, Mankame ND, Zavattieri PD. Architected material analogs for shape memory alloys. Matter 2021;4(6):1990–2012.
[13] Zhao S, Zhang Y, Zhang Y, Zhang W, Yang J, Kitipornchai S. Genetic programming-assisted micromechanical models of graphene origami-enabled metal metamaterials. Acta Mater 2022;228:117791.
[14] Yu XL, Zhou J, Liang HY, Jiang ZY, Wu LL. Mechanical metamaterials associated with stiffness, rigidity and compressibility: A brief review. Prog Mater Sci 2018;94:114–73.
[15] Zhai Z, Wu L, Jiang H. Mechanical metamaterials based on origami and kirigami. Appl Phys Rev 2021;8(4):041319.
[16] Yu T, Dreier L, Marmo F, Gabriele S, Parascho S, Adriaenssens S. Numerical modeling of static equilibria and bifurcations in bigons and. J Mech Phys Solids 2021;152:104459.
[17] Meng Z, Liu M, Zhang Y, Chen CQ. Multi-step deformation mechanical metamaterials. J Mech Phys Solids 2020;144:104095.
[18] Restrepo D, Mankame ND, Zavattieri PD. Phase transforming cellular materials. Extreme Mech Lett 2015;4:52–60.
[19] Haghpanah B, Salari-Sharif L, Pourrajab P, Hopkins J, Valdevit L. Multistable Shape-Reconfigurable Architected Materials. Adv Mater 2016;28(36):7915–20.
[20] Rafsanjani A, Akbarzadeh A, Pasini D. Snapping mechanical metamaterials under tension. Adv Mater 2015;27(39):5931–5.
[21] Correa DM, Klatt T, Cortes S, Haberman M, Kovar D, Seepersad C. Negative stiffness honeycombs for recoverable shock isolation. Rapid Prototyping Journal 2015;21:193–200.
[22] Shan S, Kang SH, Raney JR, Wang P, Fang L, Candido F, et al. Multistable Architected Materials for Trapping Elastic Strain Energy. Adv Mater 2015;27(29):4296–301.
[23] Zhu S, Wang B, Chen L, Tan X, Ma Li. Enhance the energy dissipation ability of sleeve-type negative stiffness structures via a phase-difference mechanism. Int J Mech Sci 2022;213:106803.
[24] Ma H, Wang Ke, Zhao H, Mu R, Yan Bo. A reusable metastructure for tri-directional energy dissipation. Int J Mech Sci 2022;214:106870.
[25] Zhang Y, Tichem M, van Keulen F. Concept and design of a metastructure-based multi-stable surface. Extreme Mech Lett 2022;51:101553.
[26] Che K, Yuan C, Wu J, Jerry Qi H, Meaud J. Three-dimensional-printed multistable mechanical metamaterials with a deterministic deformation sequence. J Appl Mech 2017;84:011004.
[27] Alturki M, Burgueño R. Equivalent viscous damping for a system with energy dissipation via elastic instabilities. Eng Struct 2020;220:110753.
[28] Zhang YL. Stress- and temperature-induced phase transforming Architected materials with multistable elements. Purdue University Doctor of Philosophy; 2019.
[29] Simitses G, Hodges DH. Fundamentals of structural stability. Butterworth-Heinemann 2006.
[30] Pi YL, Bradford MA. In-plane stability of preloaded shallow arches against dynamic snap-through accounting for rotational end restraints. Eng Struct 2013;56:1496–510.
[31] Liu M, Gomez M, Vella D. Delayed bifurcation in elastic snap-through instabilities. J Mech Phys Solids 2021;151:104386.
[32] Huang W, Ma C, Qin L. Snap-through behaviors of a pre-deformed ribbon under midpoint loadings. Int J Solids Struct 2021;232:111184.
[33] Qiu J, Lang JH, Slocum AH. A curved-beam bistable mechanism. J Microelectromech Syst 2004;13(2):137–46.
[34] Rafsanjani A, Pasini D. Bistable auxetic mechanical metamaterials inspired by ancient geometric motifs. Extreme Mech Lett 2016;9:291–6.
[35] Zhang Y, Restrepo D, Velay-Lizancos M, Mankame ND, Zavattieri PD. Energy dissipation in functionally two-dimensional phase transforming cellular materials. Sci Rep 2019;9:12581.
[36] Yang H, Ma L. 1D and 2D snapping mechanical metamaterials with cylindrical topology. Int J Solids Struct 2020;204:220–32.
[37] Yang H, Ma Li. 1D to 3D multi-stable architected materials with zero Poisson's ratio and controllable thermal expansion. Mater Des 2020;188:108430.
[38] Wang J-X, Liu X, Yang Q-S, Tao R, Li Y, Ma L-H. A novel programmable composite metamaterial with tunable Poisson's ratio and bandgap based on multi-stable switching. Compos Sci Technol 2022;219:109245.
[39] Ren Z, Ji L, Tao R, Chen M, Wan Z, Zhao Z, et al. SMP-based multi-stable mechanical metamaterials: From bandgap tuning to wave logic gates. Extreme Mech Lett 2021;42:101077.
[40] Qi J, Chen Z, Jiang P, Hu W, Wang Y, Zhao Z, et al. Recent Progress in Active Mechanical Metamaterials and Construction Principles. Advanced. Science 2022;9(1):2102662.
[41] Tan X, Wang B, Yao Y, Yao K, Kang Y, Zhu S, et al. Programmable Buckling-based negative stiffness metamaterial. Mater Lett 2020;262:127072.
[42] Tan X, Wang B, Zhu S, Chen S, Yao K, Xu P, et al. Novel multidirectional negative stiffness mechanical metamaterials. Smart Mater Struct 2020;29(1):015037.
[43] Korpas LM, Yin R, Yasuda H, Raney JR. Temperature-Responsive Multistable Metamaterials. Acs Appl Mater Inter 2021;13(26):31163–70.
[44] Tao R, Xi Li, Wu W, Li Y, Liao B, Liu L, et al. 4D printed multi-stable metamaterials with mechanically tunable performance. Compos Struct 2020;252:112663.
[45] Liang X, Fu H, Crosby AJ. Phase-transforming metamaterial with magnetic interactions. Proc Natl Acad Sci U S A 2022;119(1).
[46] Hua J, Lei H, Gao C-F, Guo X, Fang D. Parameters analysis and optimization of a typical multistable mechanical metamaterial. Extreme Mech Lett 2020;35:100640.